Investigation of DC-driven Glow Discharges in Subatmospheric Planar AlGaSb-Ar/He Microplasma System

Hatice Hilal YUCEL KURT * (iD) , Erhan ONGUN (iD)

Gazi University, Graduate School of Natural and Applied Sciences, Department of Physics, 06500, Ankara, Türkiye

Highlights
• Numerical analysis of DC planar semiconductor-gas discharge system.
• Spatiotemporal dynamics of fast transient gas discharge parameters.
• Bandgap tunable AlGaSb -coupled Ar/He gas discharge system.
• Infrared-to-visible wavelength conversion at micro scale.

Abstract

Various studies have been reported on the theoretical and experimental investigation of planar DC -driven gas discharge-semiconductor microplasma systems (GDSµPS) for infrared sensing and thermal image conversion applications. This conceptual research study was carried out to investigate the infrared-stimulated semiconductor-microplasma systems using the finite-element method (FEM) solver COMSOL Multiphysics DC plasma simulation program. The computational simulation study was carried out based on the boundary-separated mesh structure to visualize the spatiotemporal distribution of electron density and electron current density patterns across planar discharge cell. Numerical analyses were performed based on mixture-averaged diffusion drift theory and Maxwellian electron energy distribution function. The microplasma reactor cell was composed of a planar anode/cathode electrode pair in a two-dimensional rectangular chamber separated at a gap distance of 100 µm. A III-antimonide compound semiconductor, aluminum gallium antimonide (AlGaSb), with micron-scale digitized electron emission surface was coupled to argon/helium (Ar/He) gas medium mixed in various (%) molar fractions at 200 Torr subatmospheric pressure. The electrical equivalent circuit model was driven at 1,350 VDC. The fast transient DC glow discharges were simulated for each Ar/He gas mixture model, the spatiotemporal curves and patterns were displayed in multi-dimensional graphical media, compared, and analyzed with respect to the reference model. It is figured out that binary Ar/He gas discharge system play an important role in shaping the glow discharge characteristics of GDSµP cell for band gap tunable infrared-visible converting devices. Finally, mixing argon and helium at 30% molar fraction was proposed for the infrared-visible converter conceptual model.

1. INTRODUCTION

Several theoretical and experimental research studies have been reported in various areas of plasma science and engineering applications [1-10], including stable microplasma reactors for producing UV light sources and sensors [11]. Recent studies have also been reported on the theoretical and experimental investigation of direct current gas discharge-semiconductor microplasma systems (GDSµPS) for modeling high-efficiency infrared (IR) sensing and thermal image converting systems [12-16]. The optoelectronic properties of group III-V compound semiconductors have been investigated for a variety of applications, including high-resolution thermal imaging [17-22].

The antimonide (Sb) -rich III–V compound semiconductors, grown on GaSb or InAs substrates, include GaSb, InAs and AlSb binary compounds [23] with a wide band gap ranging from ∼0.1 to ∼1.8 eV. The diversity of accessible band alignments in III-Sb compounds is shown in Figure 1 [24] by which artificial materials with band gaps from near-infrared (IR) to far-IR can be designed.

*Corresponding author, e-mail: hkurt@gazi.edu.tr

Bandgap transitions of binary AlSb/GaSb alloys to ternary III-V compounds of $Al_xGa_{1-x}Sb$ can be controlled between an indirect band gap AlSb semiconductor with Eg = 1.62 eV and a direct band gap GaSb semiconductor with Eg = 0.72 eV depending on the specific optoelectronic application [25].
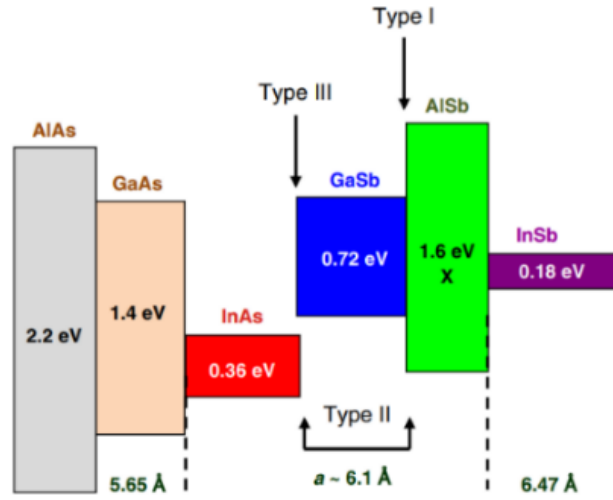

Figure 1. *Band alignments of III-As and III-Sb compounds. Scaled boxes represent band gaps of compounds, upper and lower lines of conduction and valence bands, respectively [24]*

The gas breakdown process is governed by Townsend avalanche mechanism consisting of thermionic emission, ion-induced secondary electron emission and field emission [26,27] as shown in Figure 2.
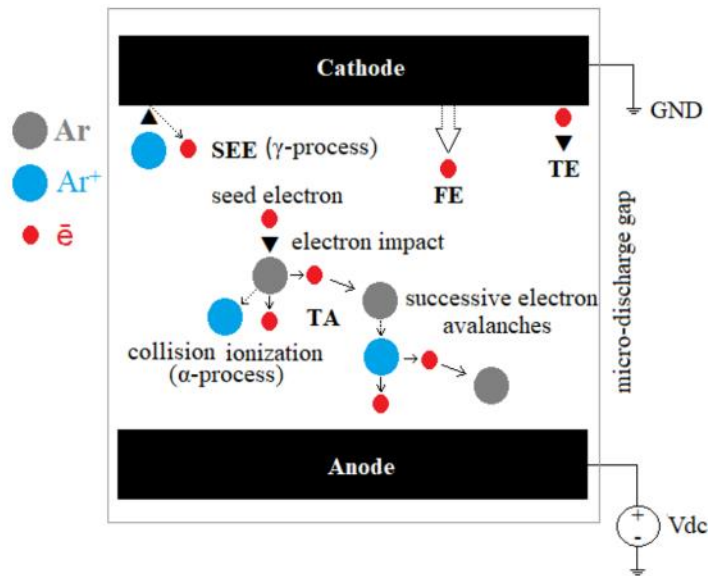

Figure 2. *Townsend avalanche (TA) mechanism of gas breakdown process. TE: thermionic emission, SEE: ion-induced secondary electron emission, FE: field emission [27]*

The gas breakdown mechanism is governed by Townsend avalanche as defined in Equation (1)

$$exp(\alpha.d) - 1 = \gamma_{SE}^{-1} \tag{1}$$

α: Ionization coeficient
d: Discharge gap distance
γ_{SE}: Secondary electron emission (SEE) coefficient.

Electrons are accelerated from the cathode to the anode. DC-field energized free electrons strike argon molecules across the micro gap, initiating the gas ionization process. Townsend avalanche mechanism drives the gas breakdown states, and the normal self-sustaining glow discharge regime is maintained under continuous infrared excitation of the photocathode. The impact of cathode surface engineering, including the growth of concentric protrusions, decoration of plasmonic metallic nanoparticles (Ag, Au), microscale patterning on the gas breakdown, and inherent surface morphology such as surface waviness and roughness on the work function has been extensively reported [28-34].

It is reported in [35] that electron energy distribution function (EEDF), which can be determined from the intensity of spectral light emissions in low-pressure helium plasmas, carries valuable information revealing the characteristics of gas discharge system. Analyzes of characteristic glow discharge light emissions (GDLE) and dependence of the discharge emission intensity (DEI) on the current in the gas medium in fast-changing plasma processes are of great importance for describing the microplasma discharge system [36].

In the scope of this research study; it is aimed to investigate the gas discharge parameters of AlGaSb semiconductor -coupled binary Ar/He gas systems for various gas mixture models. It is also aimed to obtain spatiotemporal distribution patterns of the Electron Density (ED) parameter close to the Maxwellian shape in the microplasma models.

2. MATERIALS AND METHOD

The aluminum gallium antimonide (AlGaSb) cathode electrode with micro-digitated electron emission surface was coupled to the binary argon/helium (Ar/He) gas media in various mixtures. This novel band gap tunable compound semiconductor material has been studied in this simulation model due to its high response speed, high sensitivity and efficiency in producing photons in the atmospheric window from 3 µm to 5 µm wavelength range. It is reported that Al-rich AlGaSb is more chemically stable and resistant to oxidation than pure AlSb [37,38]. The effect of process gas pressure as one of the major variable parameters in the evaluation of the microplasma discharge system has been primarily observed in the range from 150 Torr to 250 Torr. Total Ar/He gas pressure of the discharge medium was set at 200 Torr after evaluations of several simulation trials, and also referring to the experimental results [39,40].

A comprehensive study for modeling and simulation of microdischarges in the ternary AlGaSb compound semiconductor -coupled binary Ar/H_2 gas system has been recently reported in [41]. Several numerical analyzes have also been performed to investigate the spatiotemporal behavior of various compound semiconductors coupled with unary Ar and binary Ar/H_2 gas systems, exploring the transient discharge characteristics for high-efficiency infrared-to-visible wavelength conversion applications [42-44].

The simulation studies were performed using the finite-element method (FEM) solver COMSOL Multiphysics program with DC plasma module in a two-dimensional fluid model. The numerical calculations and analyses were based on mixture-averaged diffusion drift theory and Maxwellian electron energy distribution function.

Figure 3 shows a sketch of DC field-driven two-dimensional planar GDSµP (gas discharge-semiconductor microplasma) system configuration for normal glow discharges.
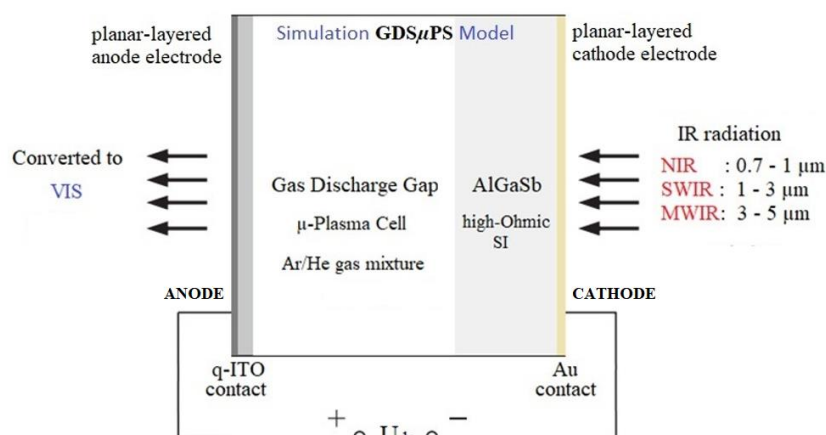
Figure 3. *DC-driven planar anode/cathode 2D-square GDSμP system configuration*

In a planar two-dimensional square chamber of GDSμP cell; the micro-digitated cathode electrode was coupled to the simple planar anode electrode across a micro gap (d). The microplasma cell was modeled to operate in the normal glow discharge regime at 200 Torr in argon-helium (Ar/He) gas medium. The electrical equivalent circuit of the cell was driven at 1,350 VDC in the simulation studies.

Figure 4 shows the electrical equivalent circuit (EEC) of gas discharge-semiconductor system used in the simulation model.
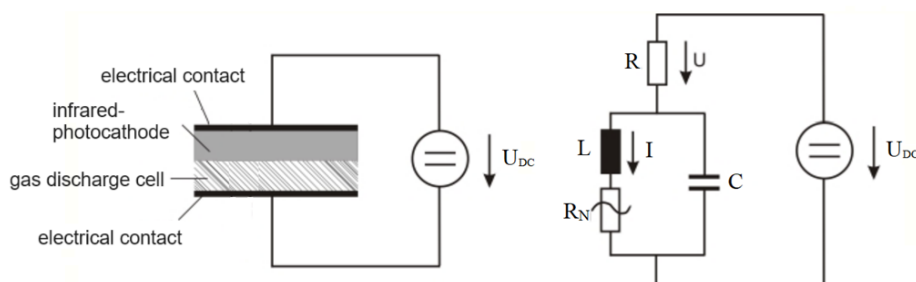

Figure 4. *The EEC of gas discharge-semiconductor system in the model (R_s=1.0 kΩ, C_p=1.0 pF)*

Simulated GDSμP system is defined by a set of parameters and variables introduced in Table 1.

Table 1. *System parameters and variables of the simulated GDSμP cell models*

Nr	System Parameters and Variables	Definitions
1	Voltage source to drive reactor cell	V=1,350 VDC
2	Process gas type	Ar/He mixtures in various ratios (Table 2)
3	Process gas pressure	P=200 Torr
4	Ambient cell operating temperature	T=300 K
5	Gas discharge gap (anode-to-cathode)	d=100 μm
6	Cathode electrode	Aluminum gallium antimonide (AlGaSb) "Ferrini, 1998: 10% Al"
7	Cathode electron emission surface	Micro-digitated in comb plate style
8	Cathode electrode radius	r=50 μm
9	Anode electrode	Indium tin oxide (ITO) coated quartz (SiO_2)
10	Initial electron density in the reactor cell	$n_{e,o}$=1.0E16 (1/m³)
11	Paschen product	P.d=200 Torr.100 μm=2,0 Torr.cm

Figure 5 shows the sketch of the GDSµP cell in the two-dimensional planar layout.
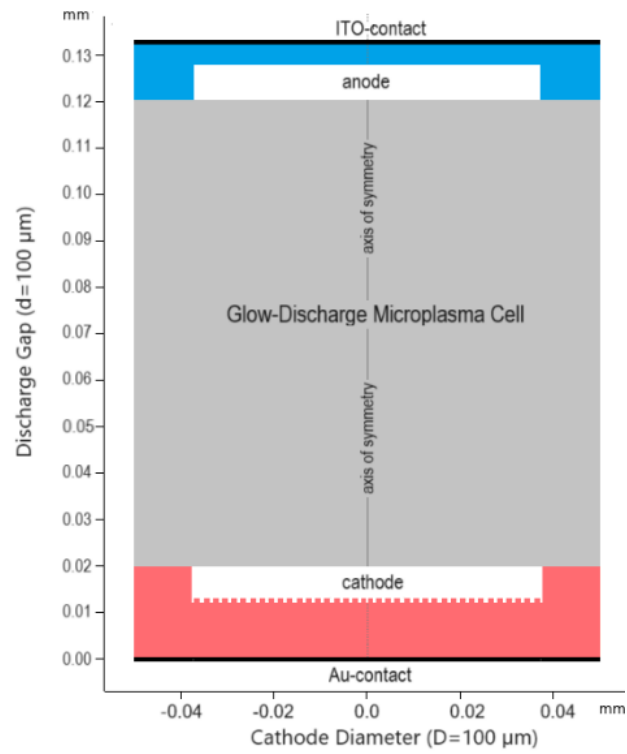

Figure 5. *Sketch of the GDSµP cell in the two-dimensional planar layout*

The computational simulation in this study was carried out based on the boundary-seperated mesh structure as shown in Figure 6 to visualize the spatio-temporal distribution of the Electron Density (ED) and the Electron Current Density (ECD) patterns in the microplasma cell.
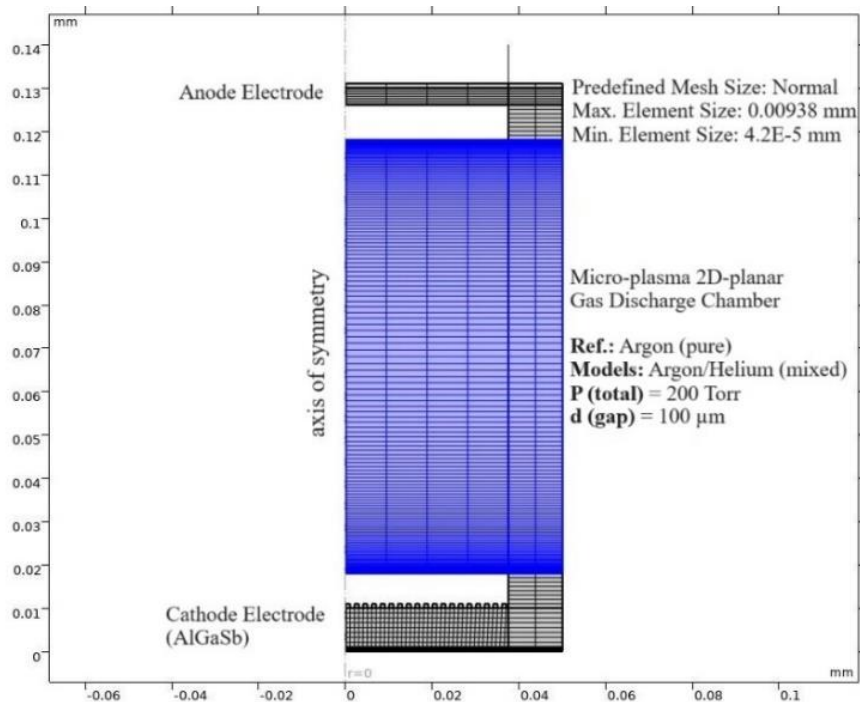

Figure 6. *Mesh structure of the two-dimensional planar GDSµP simulation cell model*

In the AlGaSb -coupled GDSμP cell simulations, a set of binary gas mixtures of Ar/He in Table 2 were individually identified, modeled and numerically analyzed. The binary Ar/He gas models were numerically compared to the reference unary Ar gas model.

Table 2. *Binary Ar/He gas mixtures (molar %) in the simulation cell models*

Model Nr.	Ar/He (x/y) mixture	Model ID
1	Ar/He (50/50)	IR-ArHe-5050
2	Ar/He (60/40)	IR-ArHe-6040
3	Ar/He (70/30)	IR-ArHe-7030
4	Ar/He (80/20)	IR-ArHe-8020
5	Ar/He (90/10)	IR-ArHe-9010
Reference	Ar/He (100/00)	IR-ArHe-0000

The fast transient DC glow micro-discharge characteristics of the AlGaSb -coupled Ar/He microplasma models were simulated from electron field emission state to self-sustained normal glow discharge state.

3. RESULTS AND DISCUSSION

The fast transient DC glow micro-discharges were simulated for each model as per defined in Table 2, the spatio-temporal 1D-curves and 2D/3D-patterns were displayed in multi-dimensional graphical media, compared and analyzed with respect to the "reference Ar/He model".

   i.   1D-spatial distribution curves of the Electron Density (ED) parameter across discharge gap in various mixtures of binary Ar/He.
   ii. 2D-spatial distribution patterns of the Electron Density (ED) parameter across discharge gap in various mixtures of Ar/He.
   iii. 3D-spatial distribution patterns of the Electron Density (ED) parameter across discharge gap in various mixtures of Ar/He.
   iv. 2D-spatial distribution patterns of the Electron Current Density (ECD) and Electron Energy Density (EED) parameters across discharge gap for the chosen mixture of Ar/He "IR-ArHe-7030 modified model" versus "the reference model".
   v.   1D-full sequence plots and 3D-spatial distribution patterns of the Electric Potential Distribution (EPD) parameter across discharge gap for the chosen mixture of Ar/He "IR-ArHe-7030 modified model" versus "the reference model".

Figure 7 shows the one-dimensional spatial and temporal variations of the Electron Density (ED) parameter across discharge gap in various mixtures of binary Ar/He gases, such as: (a) Ar/He (50/50), (b) Ar/He (60/40), (c) Ar/He (70/30), (d) Ar/He (80/20), (e) Ar/He (90/10) and (f) Ar/He (100/00) models.
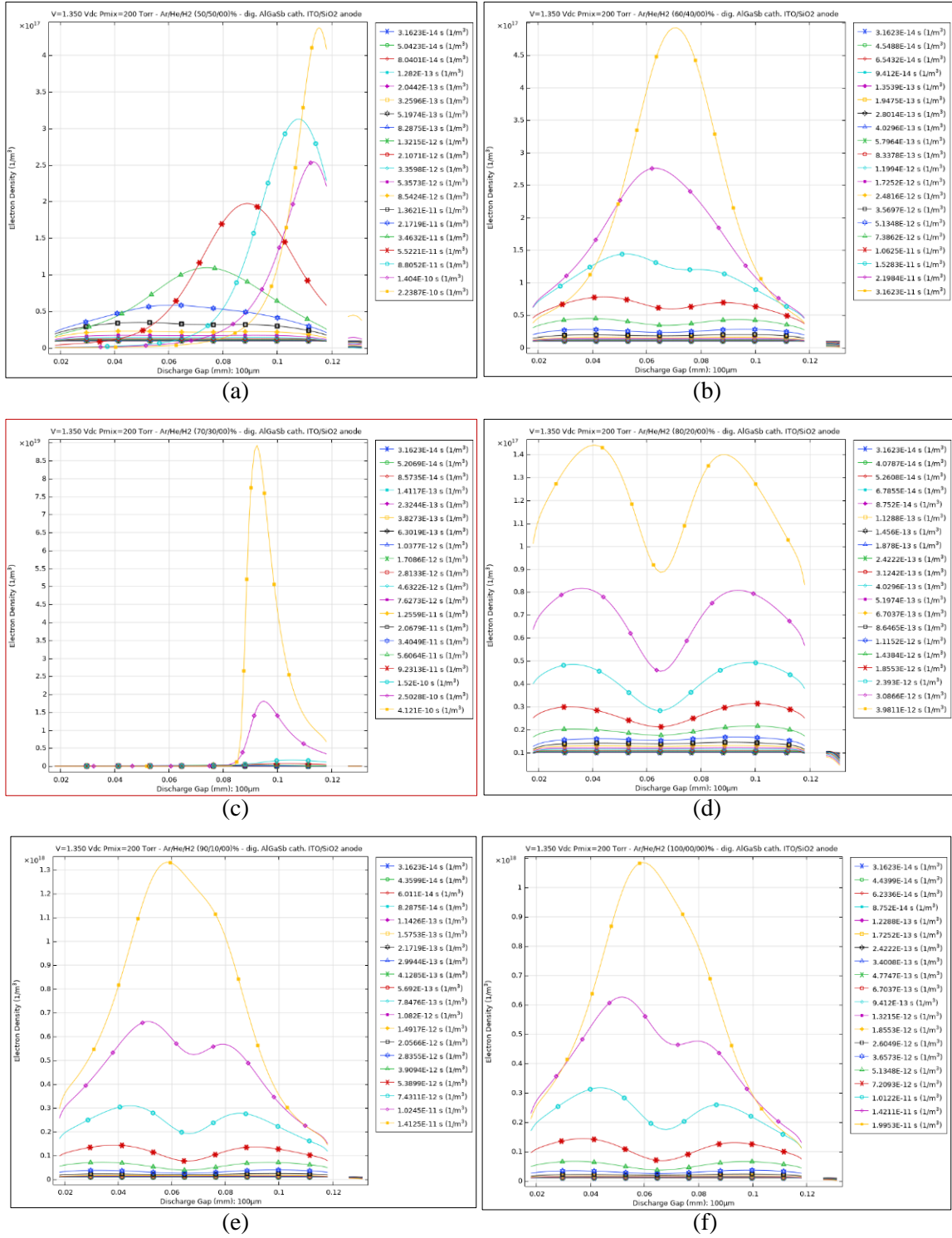
Figure 7. *1D-full phase plots of the ED parameter across discharge gap in various Ar/He mixtures: (a) ED of Ar/He (50/50), (b) ED of Ar/He (60/40), (c) ED of Ar/He (70/30), (d) ED of Ar/He (80/20), (e) ED of Ar/He (90/10), (f) ED of Ar/He (100/00)*

Numerical calculations of the ED parameter for the Ar/He (70/30) model in Figure 7 (c) reveal that one-dimensional ED distribution pattern develops much closer to the Maxwellian shape, with more localized and concentrated ED in the final phase of the microplasma process period.

Figure 8 shows the 2D-spatial distribution patterns of the Electron Density (ED) parameter calculated in the final phases of the microplasma period for respective models.
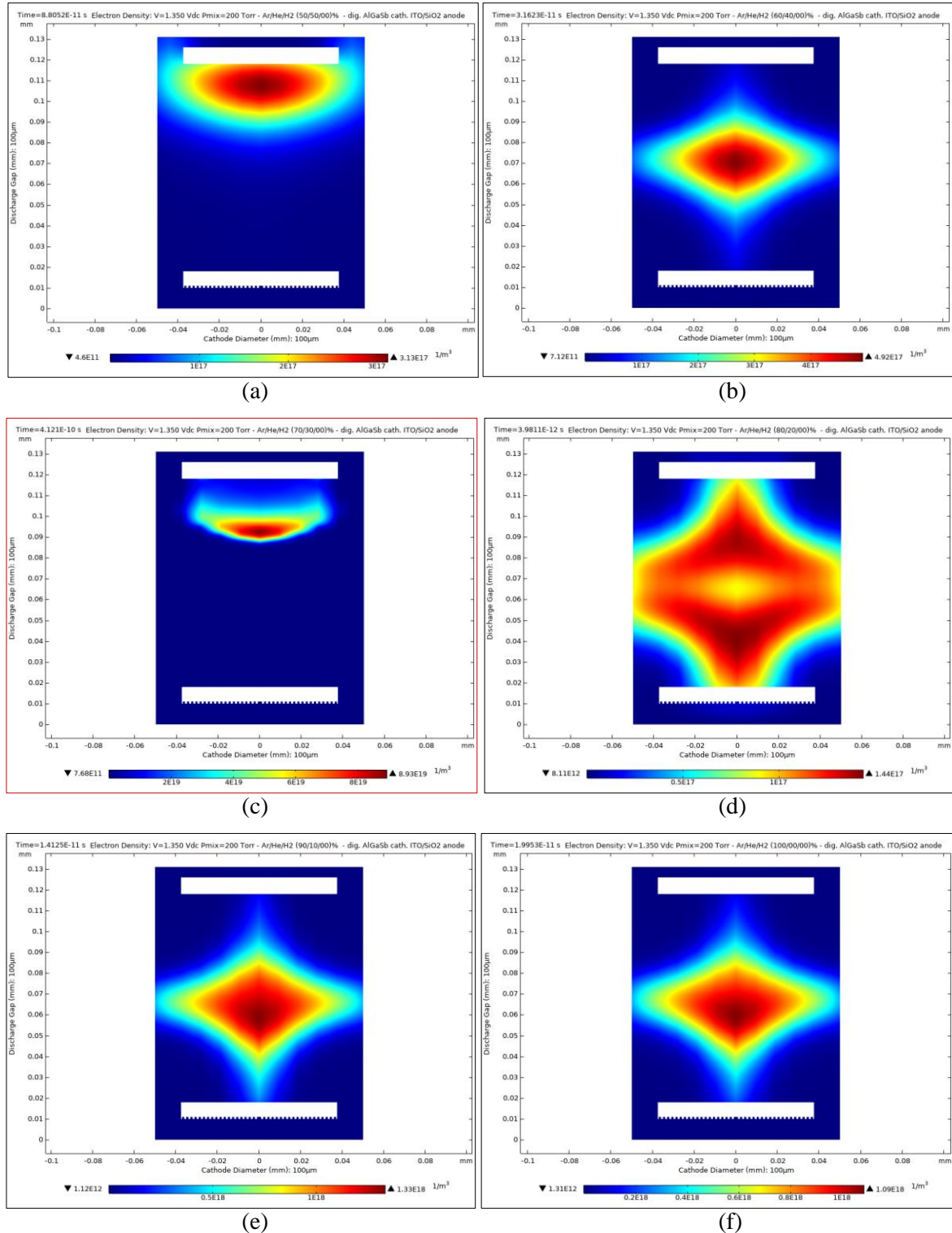

Figure 8. 2D-spatial distribution patterns of the ED parameter across discharge gap in various Ar/He mixtures: (a) ED of Ar/He (50/50), (b) ED of Ar/He (60/40), (c) ED of Ar/He (70/30), (d) ED of Ar/He (80/20), (e) ED of Ar/He (90/10), (f) ED of Ar/He (100/00) in the final phases

Figure 9 shows three-dimensional spatial distribution patterns of the Electron Density (ED) parameter calculated in the final phases of the microplasma period for respective models. Figure 9 (c) show a highly localized and concentrated 3D-ED distribution pattern in the final phase.
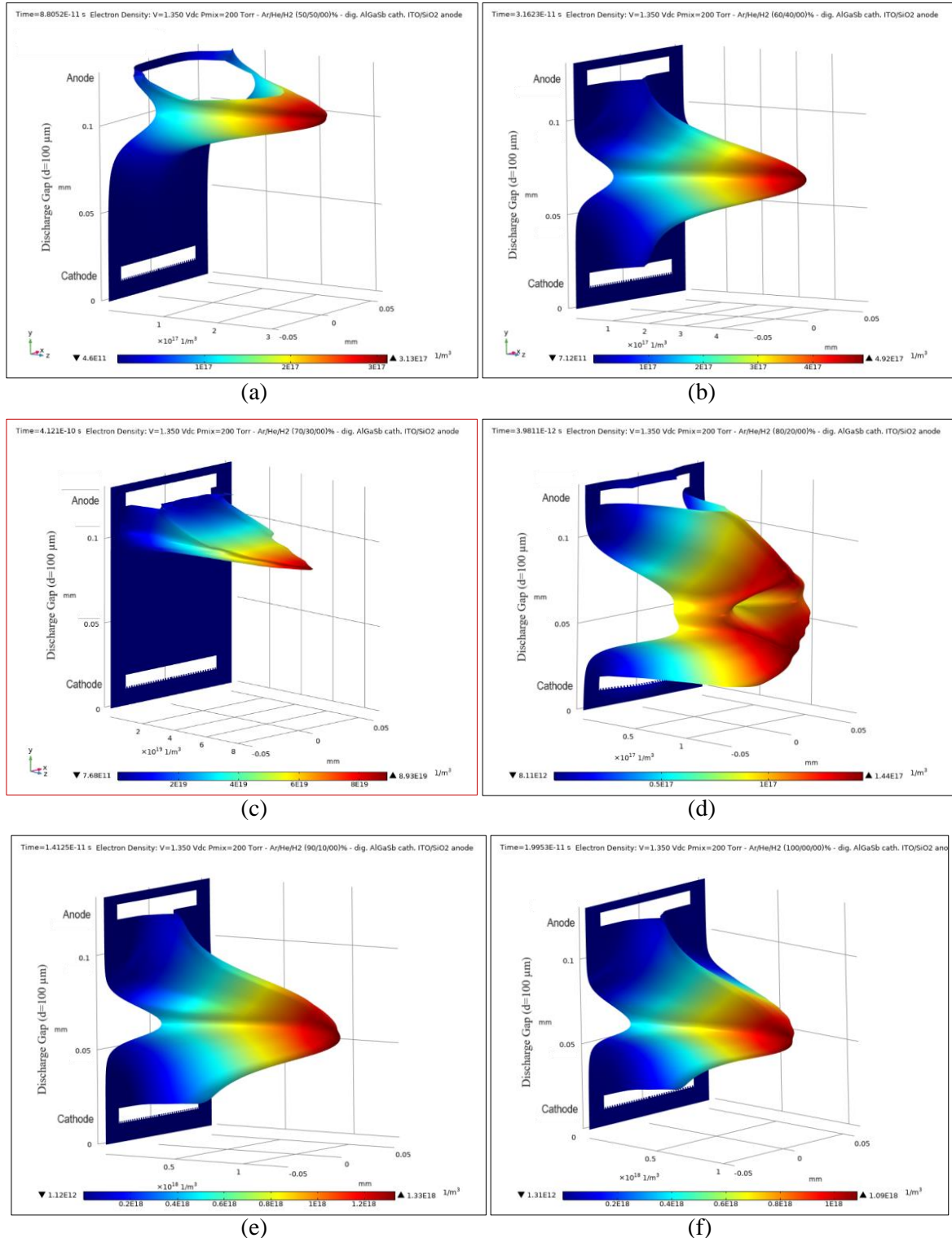

Figure 9. *3D-spatial distribution patterns of the ED parameter across discharge gap in various Ar/He mixtures: (a) ED of Ar/He (50/50), (b) ED of Ar/He (60/40), (c) ED of Ar/He (70/30), (d) ED of Ar/He (80/20), (e) ED of Ar/He (90/10), (f) ED of Ar/He (100/00) in the final phases, respectively*

The data obtained from the 3D-ED distribution patterns in Figure 9 are tabulated in Table 3.

Table 3. *All plasma models, including reference model, ED*

Ar/He (50/50)	Ar/He (60/40)	Ar/He (70/30)	Ar/He (80/20)	Ar/He (90/10)	Ar/He (100/00)
Output time_final phase (Time, s)					
8.8052E-11	3.1623E-11	4.1210E-10	3.9811E-12	1.4125E-11	1.9953E-11
Electron Density (ED, $1/m^3$)					
3.13E17	4.92E17	8.93E19	1.44E17	1.33E18	1.09E18

The chosen GDSµP cell model "Ar/He (70/30): IR-ArHe-7030" and "the reference model" were further introduced with the Electron Current Density (ECD) and the Electron Energy Density (EED) parameters in the final phases of the microplasma period in Figure 10 (a,b) and in Figure 10 (c,d), respectively.
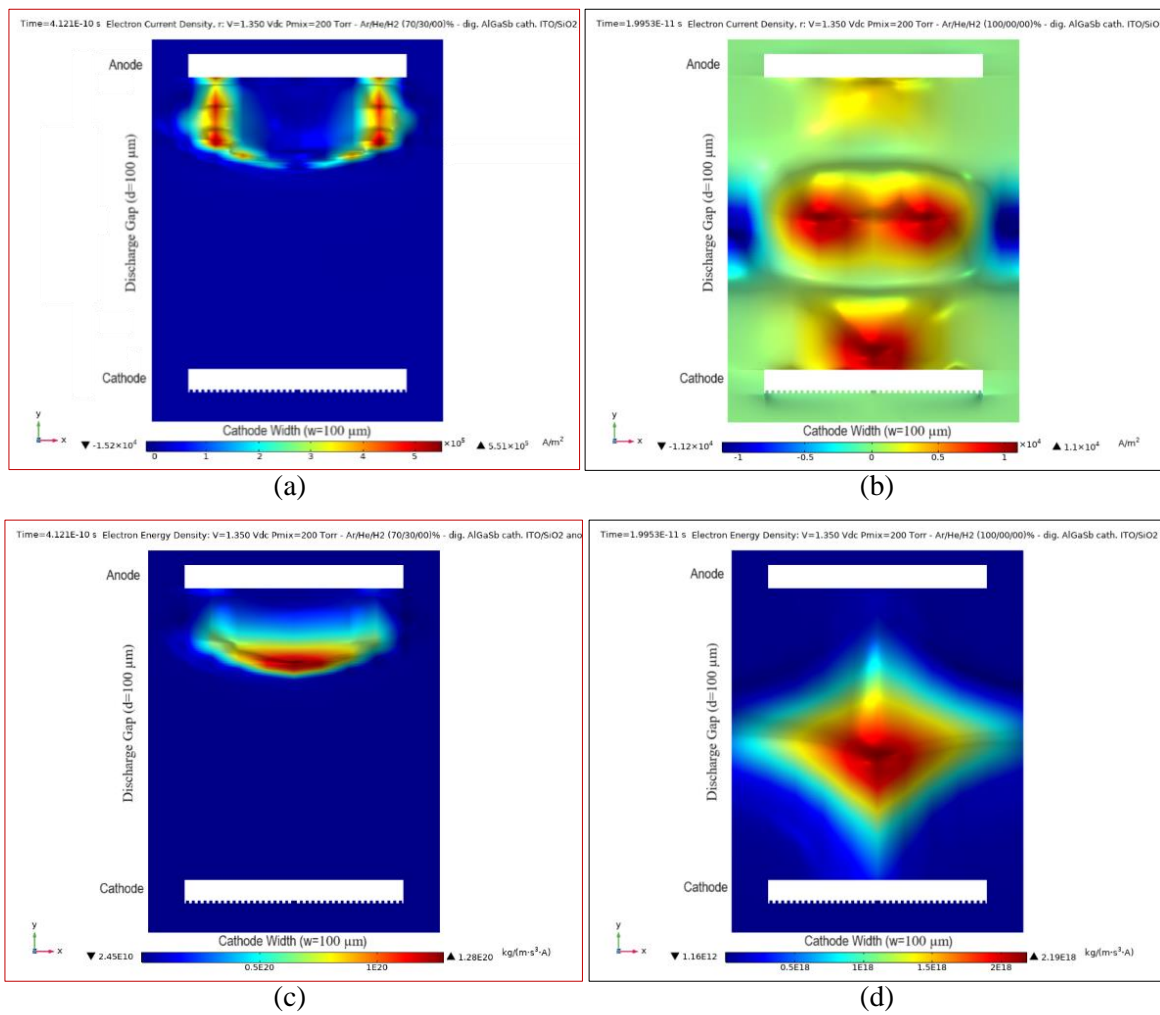

(a)

(b)

(c)

(d)

Figure 10. *2D -spatial distribution patterns of the ECD and the EED parameters across discharge gap in the chosen Ar/He mixture "IR-ArHe-7030" versus "reference model": (a) ECD of Ar/He (70/30), (b) ECD of Ar/He (100/00), (c) EED of Ar/He (70/30), (d) EED of Ar/He (100/00) in the final phases*

The data obtained from the 2D-ECD and 2D-EED patterns in Figure 10 were tabulated in Table 4.

Table 4. The chosen plasma model versus reference model, ECD and EED

Ar/He (70/30): IR-ArHe-7030	Ar/He (100/00): IR-ArHe-0000
Output time_final phase (Time, s)	
4.121E-10	1.9953E-11
Electron Current Density (ECD, A/m^2)	
5.51E5	1.1E4
Electron Energy Density (EED, kg/m s^{3}A)	
1.28E20	2.19E18

The ECD of Ar/He (70/30) model was approximately 50 times higher than that of Ar/He (100/00) reference model, while the EED of Ar/He (70/30) model was approximately 58 times higher than that of Ar/He (100/00) reference model. It was figured out that by adding helium to argon at the appropriate molar ratio, both the ECD and the EED parameters considerably enhanced. The GDSµP cell model "Ar/He (70/30): IR-ArHe-7030" and "the reference model" were further introduced with the Electric Potential Distribution (EPD) parameter in the final phases as shown in Figure 11 (a-d), respectively.
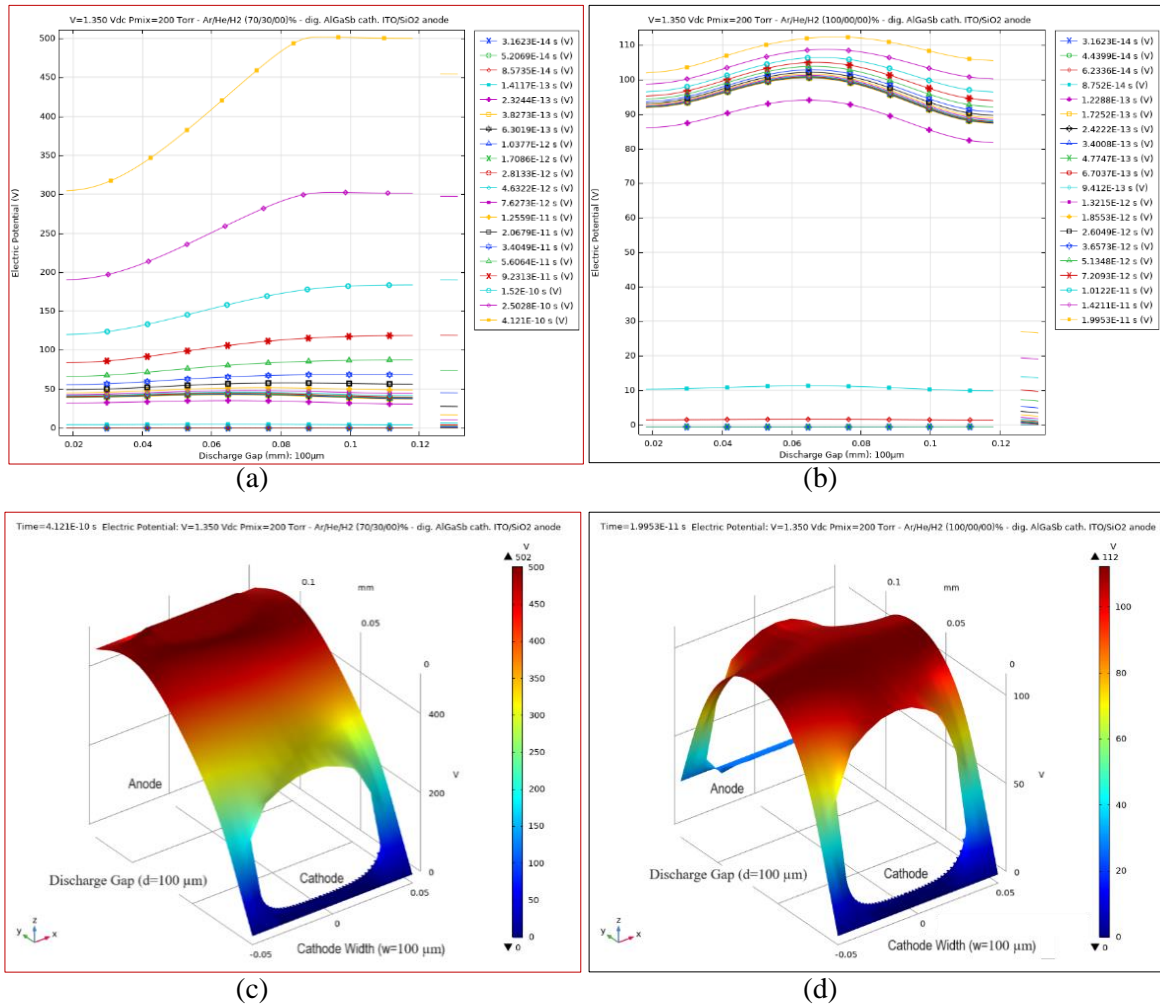

Figure 11. 1D-full process plots and 3D -spatial distribution patterns of the EPD parameter across discharge gap in the chosen Ar/He mixture "IR-ArHe-7030" versus "reference model": (a) EPD of Ar/He (70/30), (b) EPD of Ar/He (100/00), (c) EPD of Ar/He (70/30), (d) EPD of Ar/He (100/00) in the final phase

The data obtained from the 3D-EPD patterns in Figure 11 (c,d) were tabulated in Table 5.

Table 5. *The chosen plasma model versus reference model, EPD*

Ar/He (70/30): IR-ArHe-7030	Ar/He (100/00): IR-ArHe-0000
Electric Potential Distribution (EPD)	
~ 502 Vdc (at output time_final phase)	~ 112 Vdc (at output time_final phase)

It is revealed that the Electron Density (ED) parameter locally concentrates and gradually intensifies in strength in the discharge gap as the plasma reaction progresses to the final phase. The spatiotemporal intensity distribution patterns of glow discharge light emissions (GDLE) of the simulated microplasma models depend on the cell operating conditions and fraction of helium addition to argon.

Figure 12 exhibits the Paschen curves for argon and helium gases [6]. It is aimed to precisely control and locate the operating point of GDSµP cell on the imaginary vertical projection line corresponding to P.d=200 Torr.100 µm=2.0 Torr.cm on the Paschen curve by addition of helium to argon.
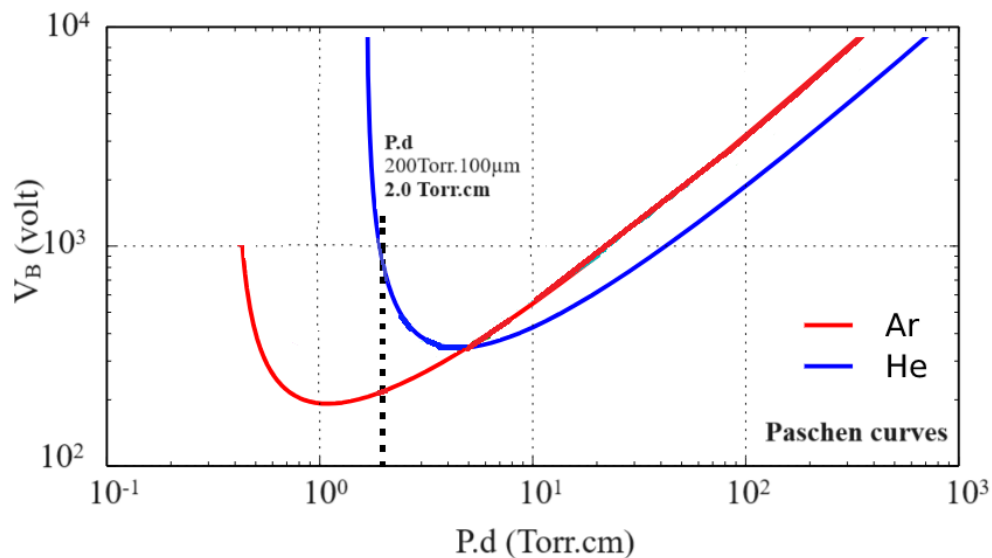

Figure 12. *Paschen curves for Ar and He[6]. The operating point of GDSµP cell on the imaginary vertical projection line corresponding to P.d=200 Torr.100 µm=2.0 Torr.cm*

Figure 13 shows the I-V characteristics curve of gas discharge system introducing "dark discharge, glow discharge and arc discharge regimes". It reveals that the calculated discharge current locates at around 0.5 mA in the normal glow discharge regime of the I-V curve. The nominal operation point of the simulated model is indicated by dashed vertical line in blue.
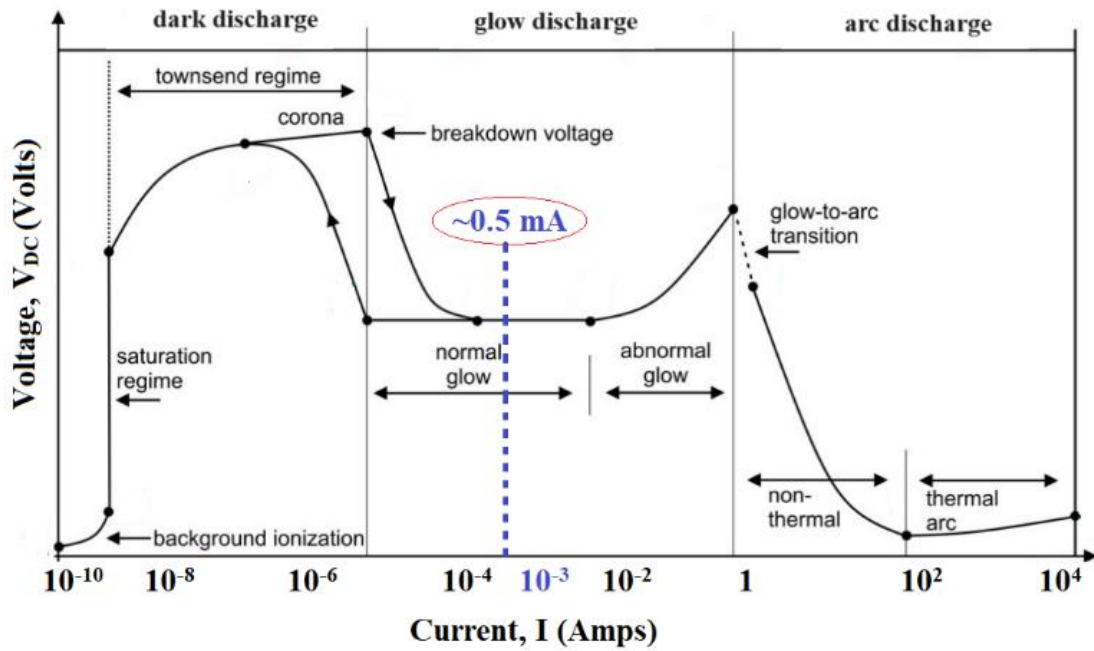
Figure 13. *Current/Voltage (I/V) curve of the gas discharge regimes [28]. The calculated discharge current of the simulated GDSμP cell locates in the normal glow discharge regime*

Protecting the cell against permanent damage due to the glow-to-arc transition is of critical importance in modeling the semiconductor-gas discharge system. A recent study on the CdS-coupled microplasma system reported that the cathode material was damaged due to the glow-to-arc transition at a discharge current of around 0.1 A [16].

4. CONCLUSION

It is figured out that binary Ar/He gas discharge systems play an important role in shaping the transitions of electro-optical properties of semiconductor-microplasma-based artificial electromagnetic media specifically configured for infrared-to-visible wavelength converting applications. The accessible band alignments of III-Sb compound AlGaSb semiconductor can be utilized to custom design wavelength-tunable artificial optoelectronic materials. A novel cathode configuration with micro-digitated electron emission surface, which is coupled to the gas discharge reactor media, can significantly improve the field emission properties and the fast changing microplasma stability of GDSμP cell.

Refering to the simulation results of the electron density (ED) parameter as displayed in Figures 7 to 9, "Ar/He (70/30): IR-ArHe-7030" cell model exhibits ED spatial distribution pattern closest to the Maxwellian shape with highly localized electron density as calculated in the final phase among the other simulated plasma models. The ECD of "Ar/He (70/30) modified model" was approximately 50 times higher than that of "Ar/He (100/00) reference model", while the EED of "Ar/He (70/30) modified model" was approximately 58 times higher than that of "Ar/He (100/00) reference model". It is figured out that by adding helium to argon at an appropriate molar ratio; the discharge parameters (ED, ECD, EED) can be significantly enhanced.

In the light of the results obtained from this study, "IR-ArHe-7030 modified model" can be proposed as a novel candidate for the infrared-visible wavelength conversion applications. However, the multi-scale understanding of the adaptive effects of all modeling tools introduced in this preliminary conceptual study needs further investigation with subsequent numerical analyses.

ACKNOWLEDGEMENT

CONFLICT OF INTEREST

No conflict of interest was declared by the authors.

REFERENCES

[1] Vossen, J. L., "Thin Film Processes", Academic Press, INC., New York, (1978).

[2] Kurt, H. Y., Kurt, E., Salamov, B.G., "Fractal processing for an analysis of the quality and resistivity of large semiconductor plates", Crystal Research and Technology 39(9): 743-753, (2004).

[3] Go, D. B., and Venkattraman, A., "Microscale gas breakdown: Ion-enhanced field emission and the modified Paschen's curve", Journal of Physics D: Applied Physics, 47: 503001, (2014).

[4] Liangliang, L., and Wang, Q., "Microplasma: A New Generation of Technology for Functional Nanomaterial Synthesis", Plasma Chemistry and Plasma Processing, 35: 925-962, (2015).

[5] Schoenbach, K. H., and Becker, K., "20 years of microplasma research: A status report", The European Physical Journal D, 70: 29, (2016).

[6] Tabib-Azar, M., Pai, P., "Microplasma Field Effect Transistors", Micromachines, 8: 117, (2017).

[7] Garner, A.L., Meng, G., Fu, Y., Loveless, A.M., Brayfield II, R.S., Darr, A.M., "Transitions between electron emission and gas breakdown mechanisms across length and pressure scales", Journal of Applied Physics, 128: 210903, (2020).

[8] Garner, A. L., Loveless, A. M., Dahal, J. N., Venkattraman, A., "A tutorial on theoretical and computational techniques for gas breakdown in microscale gaps", IEEE Transactions on Plasma Science, 48: 808-824, (2020).

[9] Chiang, W.-H., Mariotti, D., Sankaran, R. M., Eden, J. G., and Ostrikov, K., "Microplasmas for advanced materials and devices", Advanced Materials, 32(18): 1905508, (2020).

[10] Tournié, E., Bartolome, L.M., Calvo, M.R., Loghmari, Z., Díaz-Thomas, D.A., Teissier, R., Baranov, A.N., Cerutti, L., and Rodriguez, J-B., "Mid-infrared III–V semiconductor lasers epitaxially grown on Si substrates", Science & Applications, 11: 165, (2022).

[11] Wang, Q., Economou, D. J., Donnelly, V. M., "Simulation of a direct current microplasma discharge in helium at atmospheric pressure", Journal of Applied Physics, 100: 023301, (2006).

[12] Bülbül, M. M., Kurt, H. H., Salamov, B., "Surface behaviour of plasma etched photodetector in a planar gas discharge image converter", Malmö, Sweden 7th International Conference on Nanometer-Scale Science and Technology, (2002).

[13] Kurt, H. Y., Salamov, B.G., and Mammadov, T.S., "Electrical instability in a semiconductor gas discharge system", Crystal Research and Technology, 40(12): 1160-1164, (2005).

[14] Sadiq, Y., Kurt, H. Y., Albarzanji, A.O., Alekperov, S.D, Salamov, B.G., "Transport properties in semiconductor-gas discharge electronic devices", Solid-state Electronics, 53(9): 509-1015, (2009).

[15] Kurt, H. H., Koc, E., Salamov, B. G., "Atmospheric pressure DC Glow discharge in semiconductor gas discharge electronic devices", IEEE Transactions on Plasma Science, 38(2): 137-141, (2010).

[16] Kurt, H. H., Tanrıverdi, E., Salamov, B.G., "Optical and electrical properties of CdS material in a microplasma cell under IR stimulation", The Journal of The Minerals, Metals & Materials Society (JOM), 71(2): 644-650, (2019).

[17] Kurt, H.Y., Sadiq, Y., Salamov, B.G., "Nonlinear electrical characteristics of semi-insulating GaAs", Physica Status Solidi (A), 205(2): 321-329, (2008).

[18] Kurt, H.Y., Kalkan, G., Özer, M., Tanrıverdi, E., Yigit, D., "The effect of the oxidation on GaAs semiconductor surface to the system characteristics in a double-gapped plasma cell", Journal of Polytechnic, 17(4): 161-165, (2014).

[19] Kurt, H. H., Tanrıverdi, E., "The features of GaAs and GaP semiconductor cathodes in an infrared converter system", Journal of Electronic Materials, 46: 4024–4033, (2017).

[20] Kurt, H. H., Tanrıverdi, E., "Electrical properties of ZnS and ZnSe semiconductors in a plasma-semiconductor system", Journal of Electronic Materials, 46: 3965-3975, (2017).

[21] Kurt, H. H., "Exploration of gas discharges with GaAs, GaP and ZnSe electrodes under atmospheric pressure", Journal of Electronic Materials, (2018). DOI: 10.1007/s11664-018-6161-5

[22] Kurt, H. H., Salamov, B.G., "Breakdown phenomenon and electrical process in a microplasma system with InP electrode", The Journal of The Minerals, Metals & Materials Society (JOM), 72: 651–657, (2020).

[23] Guo, J., Zhao, J., Yang, M., "Interface engineering of InGaAs/InP layer for photocathode", Optik. 212, 164738, (2020).

[24] Vurgaftman, I., Meyer, J. R., Ram-Mohan, L. R., "Band parameters for III–V compound semiconductors and their alloys", Journal of Applied Physics, 89: 5815–5875, (2001).

[25] Dutta, P. S., Bhat, H. L., Kumar, V., "The physics and technology of gallium antimonide: an emerging optoelectronic material", Journal of Applied Physics, 81: 5821–5870, (1997).

[26] Ongun, E., Yücel Kurt, H.H., Utaş, S., "Investigation of direct current micro glow discharge plasma in the modified zinc selenide-argon system", 8th International Conference on Innovative Studies of Contemporary Sciences, Tokyo Summit, ISBN-978-1-955094-91-7, (2024).

[27] Yücel, H.H., Utaş, S., Ongun, E., "The study of DC- and AC-driven GaAs-coupled gas discharge micro plasma systems: Modeling and simulation", Journal of Electronic Materials, 53: 3792-3808, (2024).

[28] Ongun, E., Utaş, S., Yücel Kurt, H.H., Hançerlioğulları, A., "The investigation of spatiotemporal dynamics of planar DC field emission-driven gas discharge-semiconductor microplasma system (GDSμPS)", Turkish Physical Society 39th International Physics Congress, Bodrum Türkiye, (2023).

[29] Naresh, C. Das, "Tunable infrared plasmonic absorption by metallic nanoparticles", Journal of Applied Physics, 110: 046101, (2011).

[30] Ongun, E., "Examination of optical and metamaterial behaviours exhibited by sculptured thin-films", Master's Thesis, İstanbul Technical University, Graduate School of Natural and Applied Sciences, Materials Engineering Program, (2012).

[31] Brayfield, II R. S., Fairbanks, A. J., Loveless, A. M., Gao, S., Dhanabal, A., Li, W., Darr, C., Wu, W., and Garner, A. L., "The impact of cathode surface roughness and multiple breakdown events on microscale gas breakdown at atmospheric pressure", Journal of Applied Physics, 125: 203302, (2019).

[32] Fu, Y., Zhang, P., Krek, J., and Verboncoeur, J. P., "Gas breakdown and its scaling law in microgaps with multiple concentric cathode protrusions", Applied Physics Letters, 114: 014102, (2019).

[33] Malayter, J. R., and Garner, A. L., "Theoretical assessment of surface waviness on work function", AIP Advances, 10: 095110, (2020).

[34] Zhang, J., Wang, Y., Li, D., Sun, Y., "Engineering surface plasmons in metal/nonmetal structures for highly desirable plasmonic photodetectors", ACS Materials Letters, 4(2): 343−355, (2022).

[35] Mijović, S. and Vučeljić, Mira., "Determination of electron energy distribution function from the intensity of spectral lines by tikhonov regularization method in low pressure helium plasma", Romanian Reports in Physics, 65(4): 1384–1389, (2013).

[36] Salamov, B.G., Kurt, H. H., "Ar-driven gas discharge system based on dielectric zeolite material", The Journal of The Minerals, Metals & Materials Society (JOM), 72: 644–650, (2020).

[37] Bennett, B. R., Khan, S. A., Boos, J. B., Papanicolaou, N. A., Kuznetsov, V. V., "AlGaSb buffer layers for sb-based transistors", Journal of Electronic Materials, 39(10): 2196–2202, (2010).

[38] Bennett, B. R., Boos, J. B., Ancona, M. G., Papanicolaou, N. A., Cooke, G. A., Kheyrandish, H., "InAlSb/InAs/AlGaSb quantum well heterostructures for high-electron-mobility transistors", Journal of Electronic Materials, 36(2): 99–104, (2007).

[39] Kurt, H. H., "Exploration of the infrared sensitivity for a ZnSe electrode of an IR image converter", Journal of Electronic Materials, 47(8): 4486-4492, (2018).

[40] Kurt, H. H., "An optical method for the quality exploration of a GaAs material", Gazi University Journal of Science Part A: Engineering and Innovation GUJ Sci Part: A, 2(2): 87-98, (2014).

[41] Ongun, E., Utaş, S., Yücel Kurt, H.H., Hançerlioğulları, A., "Modeling and simulation of DC Glow discharges in the AlGaSb -coupled Ar/H_2 hybrid micro plasma system", Journal of Polytechnic, (2024). DOI: 10.2339/politeknik.1406036

[42] Ongun, E., Yücel Kurt, H.H., Utaş, S., "DC-driven subatmospheric glow discharges in the infrared-stimulated", Journal of Materials Science: Materials in Electronics, 35: 655, 1-14, (2024).

[43] Yücel, H.H., Utaş, S., Ongun, E., "The investigation of direct current microdischarges in HgCdTe-coupled Ar/H_2 gas medium at atmospheric and hyper-atmospheric pressures", Optoelectronics and Advanced Materials – Rapid Communications, 18(5-6): 296-304, (2024).

[44] Ongun, E., Yücel, H.H., "Spatiotemporal modeling and simulation of DC microplasma glow discharges in ZnSe-Ar/H_2 system", Inspiring Technologies and Innovations, 3(1): 1-8, (2024).